ADVANCED OPTICAL MATERIALS
www.advopticalmat.de

Cucurbit[8]uril Confined 6-Bromoisoquinoline Derivative Dicationic Phosphorescent Energy Transfer Supramolecular Switch for Lysosome Targeted Imaging

*Hui-Juan Wang, Wen-Wen Xing, Heng-Yi Zhang, Wen-Wen Xu, and Yu Liu**

Phosphorescent materials constructed by macrocyclic host confined guest has become a research hotspot in bioimaging. Herein, a highly efficient phosphorescent light-harvesting supramolecular switch constructed by cucurbit[8]uril (CB[8]) encapsulated dicationic 6-bromoisoquinoline derivative (G), sulfonatocalix[4]arene (SC4AD), near-infrared (NIR) fluorescence dyes, and diarylethene molecular switch (1) is reported. First, the resulting supramolecular foldamer formed by G and CB[8] works as a phosphorescent donor with phosphorescence at 605 nm. When secondary assembling with SC4AD, the phosphorescent emission peak of G⊂CB[8] generates a hypsochromic shift to 583 nm with a 6.4-fold enhancement of intensity. Further, NIR fluorescence dyes Nile Blue (NiB) and Sulfo-Cyanine 5 (cy5) are introduced to the assembly as acceptors to construct phosphorescent light-harvesting systems. As expected, light-harvesting systems with energy transfer efficiency of 57.5%/75.7% and a high antenna effect of 359.7/247.7 are constructed at an efficient donor/acceptor ratio of 100:1/15:2 for NiB and cy5, respectively. After co-assembly with diarylethene derivative (1), the phosphorescence transferred from G⊂CB[8]@SC4AD/NiB (or cy5) to 1 and caused the photoluminescence quenching after irradiation by 365 nm light. And the photoluminescence of the light-harvesting system was restored with the irradiation by >450 nm light. The highly efficient phosphorescent light-harvesting system is applied to lysosome targeted imaging in HeLa cells and information encryption.

1. Introduction

Compared to traditional fluorescent materials, room temperature phosphorescence (RTP) materials showed greater potential in the field of biological imaging, due to the nature of large Stokes shift, long lifetime, and so on.[1] However, most of the phosphorescent materials are stable in solid state but not in solution-phase due to the non-radiative relaxation decay of the triplet excited state caused by disordered molecular motions and high concentration of dissolved oxygen in solution, limiting their application in aqueous solutions.[2] To obtain RTP especially in aqueous solution, scientists have long sought to enhance the intersystem crossing (ISC) process and restrict of nonradiative decay[3] by supramolecular host-guest interaction,[4] polymerization,[5] micelle-assisted assembling,[6] heavy atom effect[7] and so on.[8] Among them, supramolecular host-guest interaction is a simple and effective strategy to achieve RTP emission in an aqueous solution. Cucurbiturils with rigid cavities can encapsulate guest molecules through noncovalent interactions to limiting the disorder molecular motions and shielding the quenchers in aqueous.[1a,9] 6-Bromoisoquinoline derivatives produced green RTP emission in aqueous solution after confined by the hydrophobic cavities of cucurbit[7]uril (CB[7]).[10] Recently, a series of RTP emission materials in aqueous media were constructed based on the host-guest interaction between 4-(4-bromophenyl) pyridine derivatives and cucurbit[8]uril (CB[8]).[1a,c,11] Despite more and more reports of RTP materials in aqueous solution, most of the phosphors show RTP emission in the visible range with shallow tissue penetration which is not conducive to biological imaging. It is still a formidable challenge to obtain RTP materials with Near-Infrared (NIR) emission in an aqueous solution. Fortunately, phosphorescence energy transfer (PET) provides a wonderful strategy to construct long-lifetime NIR emission materials.[12] Recently, Li and coworkers constructed a RTP nanoprobe with NIR afterglow based on the PET from phosphorescent molecule N,N-bis(4-methoxyphenyl)-3-methyl-4-(4,4,5,5-tetramethyl-1,3,2-dioxaborolan-2-yl) aniline (mTPA) to NIR fluorescent molecule silicon 2,3-naphthalocyanine bis(trihexylsilyloxide) (NCBS) and used for in vivo imaging.[12a] George and co-workers obtained long-lived fluorescence based on the efficient PET from bromo-substituted phthalimide derivative (CPthBr) to fluorescence dyes Sulforhodamine101 (SR101) and Sulforhodamine G (SRG) through organic-inorganic supramolecular scaffolding strategy.[13] PET shed a light to the construction of NIR luminescent materials with long lifetime. Subsequently, we constructed two phosphorescent-capturing systems with ultrahigh antenna effects (AE) and energy transfer efficiency (Φ_{ET}) via a secondary supramolecular

H.-J. Wang, W.-W. Xing, H.-Y. Zhang, W.-W. Xu, Y. Liu
Department of Chemistry
State Key Laboratory of Elemento-Organic Chemistry
Nankai University
Tianjin 300071, P. R. China
E-mail: yuliu@nankai.edu.cn

The ORCID identification number(s) for the author(s) of this article can be found under https://doi.org/10.1002/adom.202201178.

DOI: 10.1002/adom.202201178

assembly and the systems were used for lysosome imaging in cells[14] and multicolor cell labeling,[15] respectively. Although some materials with long-lifetime NIR emission were reported, it is still challengeable and essential to obtain switchable RTP material, especially with NIR emission.[16] Different from singly charged 4-(4-bromophenyl) pyridine, we herein chose dicationic 6-bromoisoquinoline derivative (**G**) and dicationic diarylethene molecular switch (**1**) to construct highly efficient phosphorescent energy transfer supramolecular switch through tightly muti-charged co-assembly. First, **G** formed supramolecular foldamer after being encapsulated by CB[8] and produced much brighter phosphorescence compared to singly charged 1-methyl-6-bromoquinolinium (**G′**). Further, amphiphilic sulfonatocalix[4]arene adorned with dodecyl groups on the lower rim (SC4AD) was introduced to supramolecular foldamer and caused a blue-shift phosphorescence at 583 nm. By virtue of the hydrophobic layer and bright phosphorescence of ternary supramolecular assembly **G**⊂CB[8]@SC4AD, two NIR dyes Nile Blue (NiB) and Sulfo-Cyanine5 (cy5) were introduced to the system as acceptors to construct highly efficient phosphorescent light-harvesting system. Notably, further co-assembly with molecular switch **1** endowed the multi-charged supramolecular assembly photo-switchable property (**Scheme 1**). This work provides a general strategy to obtain smart materials with long-lifetime NIR emission in an aqueous solution and laid foundation for the development of afterglow materials with NIR emission for in bio-imaging.

2. Results and Discussion

The guest molecule (**G**) was designed and synthesized by the conjugation of phosphor chromophore 6-bromoisoquinoline and electron donor 4-(4-methylthiophenyl) pyridinium (Scheme S1, Supporting Information) and the corresponding characterizations were shown in Figures S1–S3 (Supporting Information). Considering the donor-acceptor (D-A) structure of **G**, CB[8] with large cavity which can bind two pyridiniums and show enhanced charge transfer (CT) interaction with strong binding[4c,17] was selected as host molecule. First, we explored the stochiometric ratio between **G** and CB[8] by UV/vis absorption spectra and high mass spectrometry (HRMS). As shown in Figure S10 (Supporting Information), the MALDI-TOF-HRMS of **G**⊂CB[8] showed peak of 1777.4557 which was the signal of $[\mathbf{G}+CB[8]+H^+-2Br^-]^+$ indicating the 1:1 stochiometric ratio. And the job's plot of **G** upon complexation with CB[8] also showed the optimum binding ratio between **G** and CB[8] was 1:1 (Figure S11, Supporting Information). Further, we explored the assembly behavior of **G**⊂CB[8] by nuclear magnetic resonance (NMR). ^{1}H NMR experiments were executed to observe the interaction between **G** and CB[8] (**Figure 1**). With the addition of CB[8], the proton signals (H_{1-3}, H_6 and H_{10-13}) of **G** shifted to upfield caused by the host-shielding effect. And the protons (H_{7-9}) of the alkyl chain and methyl (H_{14}) shifted to downfield. These phenomena

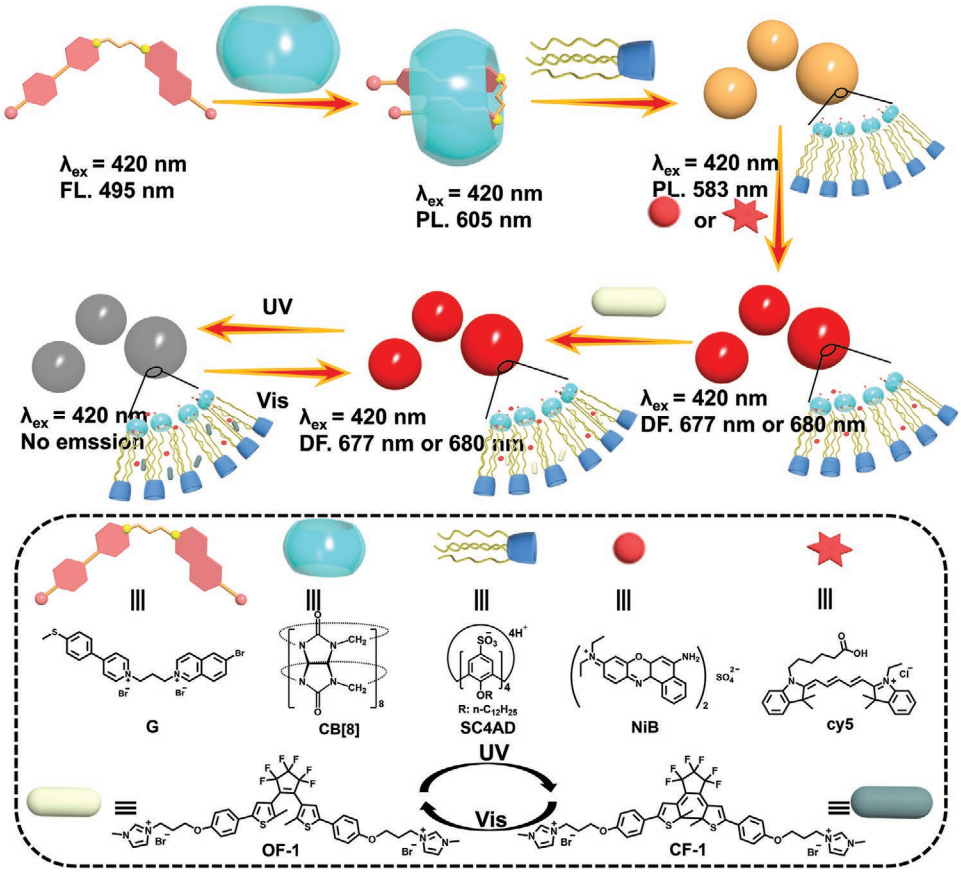

Scheme 1. Schematic diagram of the photo-switchable phosphorescent light-harvesting system (FL: fluorescent luminescence, PL: phosphorescent luminescence, DF: delayed fluorescence).

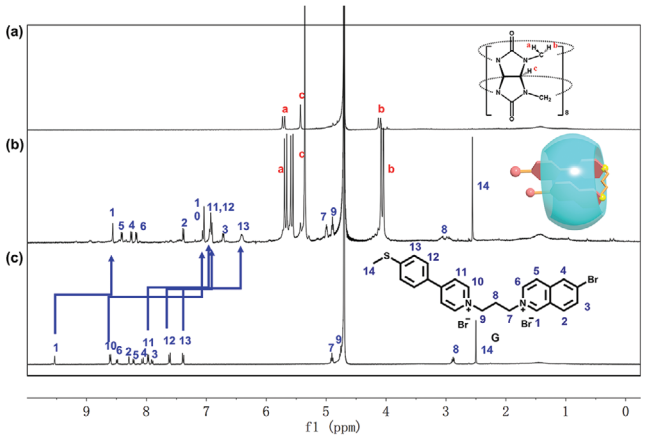

Figure 1. a) ^{1}H NMR spectra of CB[8], b) **G**⊂CB[8] and c) **G** ([CB[8]] = [**G**] = 1 mM, 400 MHz, D_2O-d_2, 298 K).

indicated that the 6-bromoisoquinoline and pyridinium moieties of **G** were included in the cavity of CB[8], while the alkyl chain and methyl of **G** were outside the cavity.[18] To further explore the binding mode of **G**⊂CB[8], 2D rotating frame overhauser effect spectroscopy (2D ROESY) NMR experiment was executed. As shown in Figure S14 (Supporting Information), the protons (H_5, H_6) of 6-bromoisoquinoline showed obvious correlations to the protons ($H_{10\text{-}12}$) of pyridinium moiety indicating the molecular folded mode of **G**⊂CB[8].

Further, the assembly behaviors of **G**⊂CB[8] were investigated by UV/vis absorption spectra. As shown in **Figure 2**a, the UV/vis absorption spectrum of **G** showed obvious absorbance peaks at 245 nm and 368 nm. With the addition of CB[8], the UV/vis absorbance peak of **G** generated an obvious bathochromic shift from 368 nm to 420 nm, which means the guest molecule **G** was encapsulated into the cavity of CB[8]. This phenomenon indicated that the assembly of **G**⊂CB[8] formed an efficient CT effect. The phosphor chromophore 6-bromoisoquinoline moiety of **G** acted as electron acceptor and 4-(4-methylthiophenyl) pyridinium moiety acted as electron donor. Subsequently, the UV/vis absorbance intensities of **G** with different concentrations of CB[8] at 420 nm were recorded and the binding constant (K_S) between CB[8] and **G** was calculated as 9.7×10^6 M^{-1} (Figure 2a, inset). Further, the assembly behaviors of **G**⊂CB[8] were investigated by transmission electron microscopy (TEM) images and dynamic light scattering (DLS). We found that the guest molecule can self-assemble into uniform nanoparticles, but the complex with CB[8] can form larger nanoparticle with a diameter of dozens of nanometers (Figure S15, Supporting Information).

Subsequently, the photophysical properties of **G**⊂CB[8] were characterized by steady-state photoluminescence spectra. The aqueous solution of guest molecule **G** showed weak fluorescence emission at 495 nm upon 420 nm light excitation with a lifetime of 1.32 ns (Figure S16, Supporting Information). As shown in Figure 2b, with the gradually addition of CB[8], the fluorescence emission peak of **G** at 495 nm decreased gradually

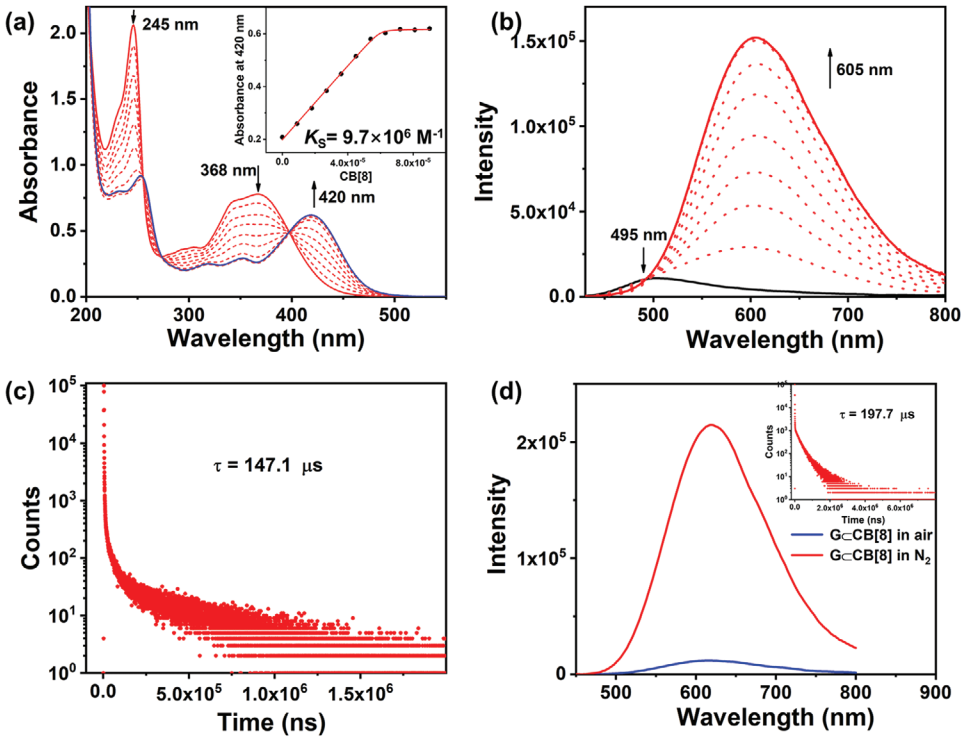

Figure 2. a) UV/vis absorption spectra of **G** (4.5×10^{-5} M) with different concentrations of CB[8] ranging from 0 to 9×10^{-5} M in aqueous solution (inset: nonlinear least-squares fit of the absorption changes at 420 nm of **G** upon addition of CB[8]). b) Steady state spectra of **G** (3×10^{-5} M) with different concentrations of CB[8] (0–6×10^{-5} M, λ_{ex} = 420 nm, 298 K). c) Time-resolved photoluminescence decay curve of **G**⊂CB[8] at 605 nm. d) Phosphorescence emission spectra (delayed 50 μs) of **G**⊂CB[8] under ambient conditions (blue curve) and in nitrogen (red curve). Inset: Time-resolved photoluminescence decay curve of **G**⊂CB[8] in nitrogen at 605 nm.

until disappeared and a new emission peak at 605 nm appeared and increased quickly. Considering the RTP emission of 6-bromoisoquinoline in the rigid microenvironment,[10] the transient emission spectra (delayed 50 μs) of **G** with different concentrations of CB[8] were measured. Figure S17, Supporting Information, showed that there were no signals for **G** and the delayed emission at 605 nm appeared and increased with the addition of CB[8]. To further confirm the photophysical properties of the delayed emission of **G**⊂CB[8] at 605 nm, the time-resolved photoluminescence decay curve of **G**⊂CB[8] at 605 nm was measured and the result showed a lifetime of 147.1 μs (Figure 2c). Further, the delayed emission spectra of the aqueous solution of **G**⊂CB[8] before and after being degassed by nitrogen ball were measured. As shown in Figure 2d, the emission intensity of **G**⊂CB[8] at 605 nm generated an obvious increase and the lifetime increased to 197.7 μs after being degassed by a nitrogen ball. To confirm the photophysical property of the emission at 605 nm, the steady-state spectra and delayed spectra of **G**⊂CB[8] at different temperatures were measured and the intensity of emission showed an obvious increasement with the decline of temperature (Figure S20, Supporting Information). These results indicated that the emission at 605 nm could be classified as RTP emission in an aqueous solution. Guest molecule **G** can be formed as molecular foldamer after being encapsulated by CB[8] with enhanced charge transfer which can reduce the energy gap between singlet and triplet and promote phosphorescence.[4c] As a reference, the delayed emission spectra of **G′**, **G′**⊂CB[8], **G″** and **G″**⊂CB[8]were measured and showed almost no phosphorescence emission (Figure S18, Supporting Information) which further indicated that the CB[8] confined supramolecular foldamer is an efficient strategy to induce the phosphorescence of 6-bromoquinolinium.

In order to press forward on deeper research on the photophysical property of **G**⊂CB[8], amphiphilic compound sulfonatocalix[4]arene adorned with dodecyl groups on the lower rim (SC4AD)[19] was introduced to form a ternary supramolecular assembly. Delayed emission spectra (delayed 50 μs) of **G**⊂CB[8] with different concentrations of SC4AD were measured. As shown in **Figure 3**a, with the gradual addition of SC4AD, the phosphorescence emission peak of **G**⊂CB[8] generated blueshift to 583 nm and the intensity increased obviously (nearly 6.4-fold of original intensity) in aqueous solution. The addition of SC4AD enhanced the hydrophobicity of microenvironment of **G**⊂CB[8] which may lower the polarity and further cause the blue-shift of phosphorescence emission peak. Further, time-resolved photoluminescence decay curve of **G**⊂CB[8]@SC4AD at 583 nm was measured and showed a lifetime of 200.7 μs (Figure 3a, Inset). The photoluminescence intensity of **G**⊂CB[8]@SC4AD at 583 nm increased greatly after being degassed by nitrogen ball (Figure S19, Supporting Information). The introduction of SC4AD can form aggregates to further limit the rotation of molecules and provide a hydrophobic environment[20] to avoid the quenching of the excited triplet state in water.[14] All these phenomena indicated that the enhanced emission at 583 nm was attributed to phosphorescence. In addition, the phosphorescence quantum yield of **G**⊂CB[8] was measured as 2.4% and increased to 7.9% after secondary assembly with SC4AD. To further investigate the ternary supramolecular assembly **G**⊂CB[8]@SC4AD, TEM and DLS experiments were executed. The results showed that **G**⊂CB[8]@SC4AD formed homogeneous nanoparticles with a diameter of 122.3 nm (Figure S15, Supporting Information).

Considering the hydrophobic layer and outstanding phosphorescence properties, the ternary supramolecular assembly **G**⊂CB[8]@SC4AD was used as a donor to construct artificial light-harvesting system based on phosphorescence energy transfer (PET)[12a] from phosphors to NIR fluorophores (Figure 3g). To achieve efficient PET, two conditions should be meet: a) close spatial distance between donor and acceptor, b) the absorption spectrum of acceptor should match with the phosphorescent spectrum of donor. As shown in Figure 3g, the electrostatic interaction and hydrophobic microenvironment caused by SC4AD closed the distance between donor and acceptor, making the energy transfer from the triplet of donor to the singlet of acceptor possible. We chose two NIR emitting dyes Nile Blue (NiB) and Sulfo-Cyanine5 (cy5) as acceptors which can be loaded by **G**⊂CB[8]@SC4AD through both electrostatic and hydrophobic interactions. As shown in Figure 3b, the absorbance spectra of both NiB and cy5 showed good overlap with the phosphorescence spectrum of **G**⊂CB[8]@SC4AD. With the gradual addition of NiB to the aqueous solution of **G**⊂CB[8]@SC4AD, the phosphorescence intensity at 583 nm decreased and a delayed emission of NiB at 677 nm increased obviously upon excitation at 420 nm (Figure 3c). More interestingly, the red-emission of NiB was readily observed even adding a trace amount of NiB (donor/acceptor = 1800:1). Until the ratio of donor/acceptor reached 100:1, the intensity of emission at 677 nm was no more enhancement. The time-resolved photoluminescence decay curve of **G**⊂CB[8]@SC4AD/NiB (donor: acceptor = 100:1) at 677 nm was measured and showed the lifetime of 77.7 μs (Figure S21, Supporting Information). While the life-time of **G**⊂CB[8]@SC4AD/NiB at 583 nm was reduced to 94.3 μs which indicated the phosphorescence energy transfer from triplet to singlet.[21] Also, the delayed emission peak at 677 nm ascribed to NiB in the light-harvesting system (**G**⊂CB[8]@SC4AD/NiB) was in line with the fluorescence peak of NiB (Figure S22a, Supporting Information), indicating the delayed fluorescence photophysical property. Similarly, an obvious decrease of the intensity at 583 nm and a gradually increased red-emission at 680 nm was observed when adding cy5 to the aqueous solution of **G**⊂CB[8]@SC4AD (Figure 3e). The emission at 680 nm belonging to cy5 in **G**⊂CB[8]@SC4AD/cy5 system attained a maximum when the donor: acceptor reach 15:2 and was identical to the fluorescence peak of cy5 (Figure S22b, Supporting Information), indicating its delayed fluorescence nature. The lifetime of the delayed fluorescence of **G**⊂CB[8]@SC4AD/cy5 (donor/acceptor = 15:2) at 680 nm was measured as 69.7 μs (Figure S21, Supporting Information). Energy transfer efficiency (Φ_{ET}) and antenna effect (AE) are two important factors to evaluating light-harvesting system. As shown in Figure 3d, the Φ_{ET} of **G**⊂CB[8]@SC4AD/NiB system was calculated as 57.5% and the AE was found to be 359.7 with a donor/acceptor ratio of 100:1. When it comes to cy5, the Φ_{ET} of **G**⊂CB[8]@SC4AD/cy5 system was calculated as 75.7% and the AE was found to be 247.7 at an efficient donor/acceptor ratio of 15:2 (Figure 3f). Further similar experiments were executed with **G**⊂CB[8] and there were no PET occurred

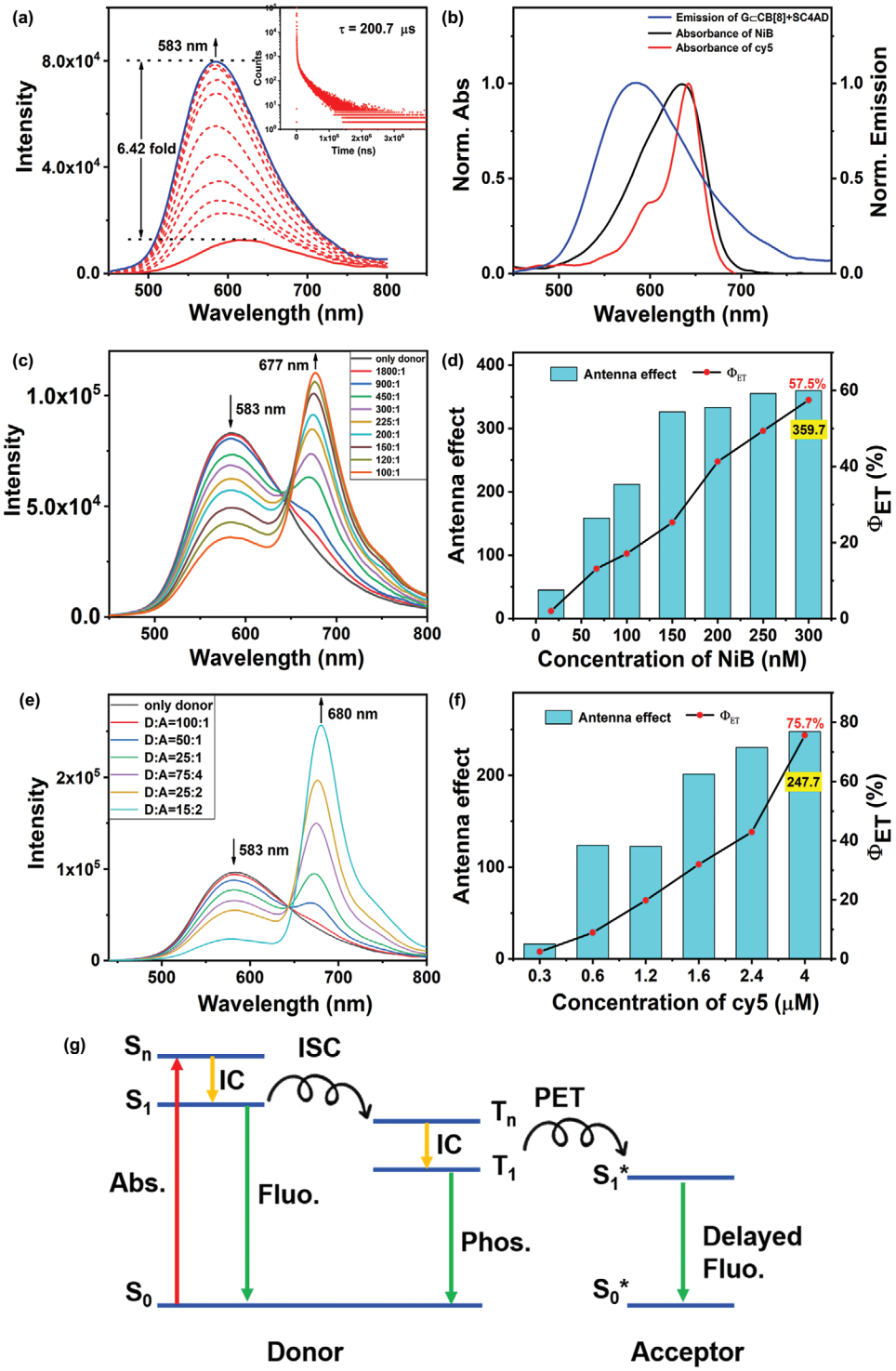

Figure 3. a) Phosphorescence emission spectra (delayed 50 μs) of **G**⊂CB[8] with different concentration of SC4AD (0–60 μM). Inset: Time-resolved photoluminescence decay of **G**⊂CB[8]@SC4AD at 583 nm. b) Normalized photoluminescence emission spectrum of **G**⊂CB[8]@SC4AD and absorption spectra of NiB and cy5, c,e) phosphorescence emission spectra (delayed 50 μs) and d,f) antenna effect/Φ_{ET} of **G**⊂CB[8]@SC4AD/NiB and **G**⊂CB[8]@SC4AD/cy5 at different donor/acceptor ratios in aqueous solution ([**G**] = 3×10^{-5} M, [CB[8]] = 3×10^{-5} M, [SC4AD] = 6×10^{-5} M, λ_{ex} = 420 nm). g) Possible mechanism diagram of the phosphorescence energy transfer (PET) process (Abs. = absorption, Fluo. = fluorescence, Phos. = phosphorescence, ISC = Intersystem crossing, IC = internal conversion).

between donor (**G**⊂CB[8]) and acceptors (NiB or cy5) indicated the essential of secondary assembly for PET (Figure S27, Supporting Information).

To obtain a photo-switchable light-harvesting system, a diarylethene derivative **1** was synthesized in open form (OF-**1**) through the route shown in Scheme S2, Supporting Information,

and the corresponding characterizations were given in Figures S4–S9 (Supporting Information). First, the photoreaction yield of **1** was investigated by ^{1}H NMR spectra. As shown in Figure S28, the protons (H_i, H_j, and H_k) of **1** shifted to downfield and the proton H_j of **1** shifted to upfield after irradiation with 365 nm light for 120 minutes and the results indicated 78.1% OF-**1** transformed to CF-**1**. Further, irradiation with >450 nm light the proton signals of CF-**1** changed back to their original position. Then the photoreaction of **1** was investigated by UV/vis spectra. The aqueous solution of OF-**1** showed a sharp absorption peak at 300 nm, after irradiation with 365 nm light, the absorption at 300 nm decreased and a new peak at 600 nm appeared and increased rapidly indicating the formation of a closed form of **1** (CF-**1**) (Figure S29a, Supporting Information).[22] Subsequently, the solution of CF-**1** was irradiated by >450 nm light and the absorption at 600 nm decreased until disappeared (Figure S29b, Supporting Information). Considering that the absorbance spectrum of CF-**1** showed good overlap to the photoluminescence spectra of **G**⊂CB[8]@SC4AD/NiB and **G**⊂CB[8]@SC4AD/cy5 (**Figure 4**a,d), compound **1** was introduced to the light-harvesting system as an acceptor. As expected, the photoluminescence of **G**⊂CB[8]@SC4AD/NiB at 678 nm decreased with irradiation of 365 nm light and recovered partially with irradiation of >450 nm light in the presence of **1** (Figure 4b,c). When it comes to **G**⊂CB[8]@SC4AD/cy5, a similar phenomenon at 680 nm was observed (Figure 4e,f). A photo-switchable phosphorescent light-harvesting system was constructed. Finally, the solution of **G**⊂CB[8]@SC4AD, **G**⊂CB[8]@SC4AD+NiB, and **G**⊂CB[8]@SC4AD+NiB+**1** were dropped into the holes of 96 hole plate to consisted of alphabets "N", "K" and "U" respectively. As shown in Figure 4g, under the excitation of 365 nm light, the 96 hole plate showed the information of "NKU" and changed to "NK" after irradiation by 365 nm UV light for several minutes. Interestingly, further irradiation by >450 nm visible light the information recovered to "NKU".

Benefiting from the outstanding phosphorescent capture characteristics of the artificial light-harvesting system, **G**⊂CB[8]@SC4AD/NiB and **G**⊂CB[8]@SC4AD/cy5 were applied to NIR cell imaging using HeLa cells as model. First, we tested the cytotoxicity of the artificial light-harvesting system by Cell Counting Kit-8 (CCK-8) assays. HeLa cells were incubated with **G**⊂CB[8]@SC4AD/NiB and **G**⊂CB[8]@SC4AD/cy5 for 24 hours before adding CCK-8, respectively. The test results

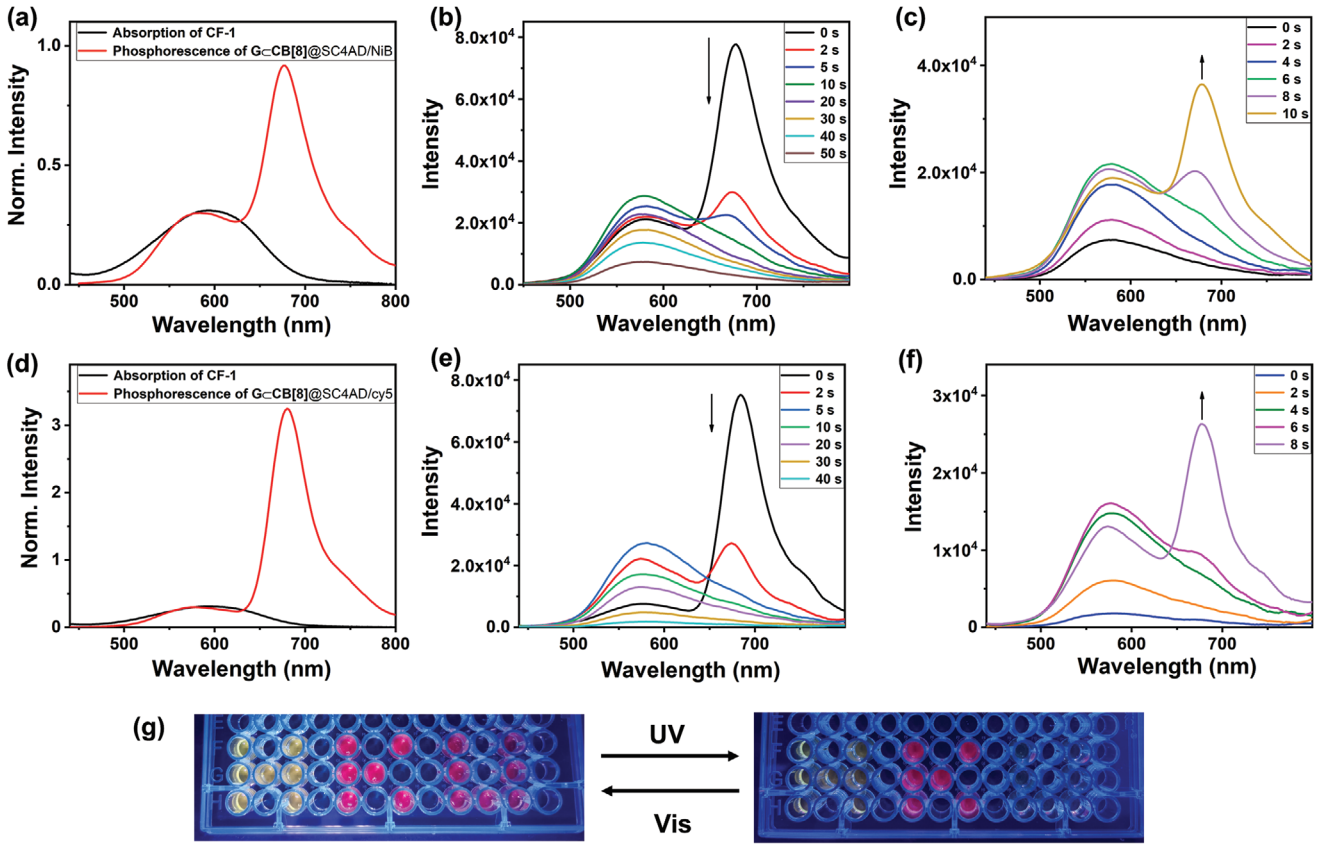

Figure 4. a) Normalized phosphorescence emission spectra (delayed 50 μs) of **G**⊂CB[8]@SC4AD+NiB and absorption spectrum of CF-**1**. b) Photoluminescence emission spectrum of **G**⊂CB[8]@SC4AD+NiB+OF-**1** with 365 nm light irradiation for different time. c) Photoluminescence emission spectrum of **G**⊂CB[8]@SC4AD+NiB+CF-**1** with >450 nm light irradiation for different time. d) Normalized phosphorescence emission spectra (delayed 50 μs) of **G**⊂CB[8]@SC4AD+cy5 and absorption spectrum of CF-**1**. e) Photoluminescence emission spectra of **G**⊂CB[8]@SC4AD+cy5+OF-**1** with 365 nm light irradiation for different time. f) Photoluminescence emission spectra of **G**⊂CB[8]@SC4AD+cy5+CF-**1** with >450 nm light irradiation for different time. ([**G**] = [**1**] = 3×10^{-5} M, [CB[8]] = 3×10^{-5} M, [SC4AD] = 6×10^{-5} M, [NiB] = 3×10^{-7} M, [cy5] = 4×10^{-6} M, λ_{ex} = 420 nm). g) Photographs of information encryption based on switchable phosphorescent light-harvesting system (N:**G**⊂CB[8]@SC4AD, K:**G**⊂CB[8]@SC4AD+NiB, U:**G**⊂CB[8]@SC4AD+NiB+**1**).

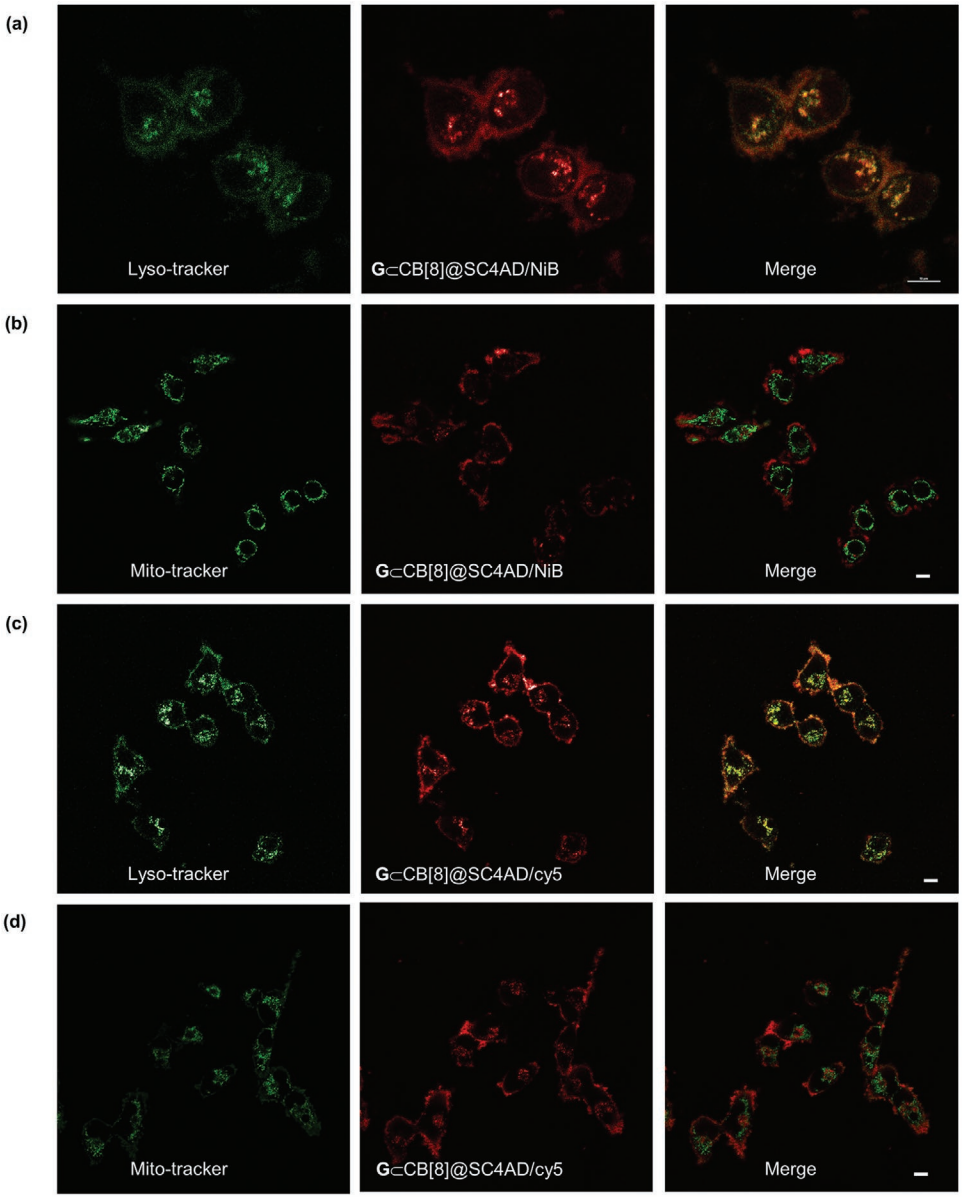

Figure 5. Confocal laser scanning microscopy images of Hela cells co-stained with **G**⊂CB[8]@SC4AD/NiB and a) Lyso Tracker Green, b) Mito Tracker Green, respectively. Confocal laser scanning microscopy images of Hela cells co-stained with **G**⊂CB[8]@SC4AD/cy5 and c) Lyso Tracker Green, d) Mito Tracker Green, respectively. The emission of Lyso/Mito Tracker Green was obtained using excitation at 405 nm by green channel. The emission of **G**⊂CB[8]@SC4AD+NiB/cy5 was obtained using excitation at 405 nm by red channel ([**G**] = 3×10^{-5} M, [CB[8]] = 3×10^{-5} M, [SC4AD] = 6×10^{-5} M, [NiB] = 3×10^{-7} M, [cy5] = 4×10^{-6} M). Scale bar: 10 μm.

indicated that both **G**⊂CB[8]@SC4AD/NiB and **G**⊂CB[8]@SC4AD/cy5 showed insignificant toxicity to HeLa cells even the concentration reached to 50 μM (Figure S30, Supporting Information). To examine the intracellular light-harvesting, HeLa cells were incubated with **G**⊂CB[8]@SC4AD/NiB for 12 h respectively and then co-stained with commercial staining dyes Lyso Tracker and Mito Tracker before being tested by confocal laser scanning microscopy (CLSM). As shown in **Figure 5**a, the red emission of **G**⊂CB[8]@SC4AD/NiB showed good overlap with the green emission of Lyso Tracker with a high Pearson's correlation coefficient of 0.91 (Figure S31a, Supporting Information). When it turns to Mito Tracker, there was almost no overlap between red emission and green emission (Figure 5b), indicating that the **G**⊂CB[8]@SC4AD/NiB targeted imaging in lysosomes rather than mitochondria. In addition, colocalization assays were executed to observe the subcellular distribution of **G**⊂CB[8]@SC4AD/cy5. The HeLa cells were incubated with **G**⊂CB[8]@SC4AD/cy5 for 12 h and then co-incubated with commercial dyes (Lyso Tracker and Mito Tracker, respectively) before being examined by CLSM. As shown in Figure 5c, the red emission of **G**⊂CB[8]@SC4AD/cy5 showed excellent overlap with the green emission of Lyso Tracker (Pearson's correlation coefficient of 0.92, Figure S31b) and very little overlap with the green emission of Mito Tracker (Figure 5c,d). These results indicated that **G**⊂CB[8]@SC4AD/cy5 accumulated in lysosomes first.

3. Conclusion

In summary, an artificial light-harvesting system with excellent phosphorescence capturing character was constructed by the co-assembly of **G**, CB[8], and SC4AD. Guest molecule **G** consisted of electron donor 4-(4-methylthiophenyl) pyridinium and phosphor chromophore 6-bromoisoquinoline. CB[8] could binding with equivalent **G** to form supramolecular foldamer accompanying the transformation of fluorescence at 495 nm to phosphorescence at 605 nm. Further assembling with SC4AD, the phosphorescence emission peak of **G**⊂CB[8] blue shift to 583 nm and showed an obvious enhancement. The ternary supramolecular assembly **G**⊂CB[8]@SC4AD can form nanoparticles with an average diameter of 122.3 nm and displayed fantastic potential in constructing artificial light-harvesting system in an aqueous solution. Two NIR dyes (NiB and cy5) were introduced to **G**⊂CB[8]@SC4AD respectively and acted as acceptors in the process of PET. Interestingly, light-harvesting systems with energy transfer efficiency (Φ_{ET}) of 57.5% and high antenna effect (AE) of 359.7 for NiB (for cy5: Φ_{ET} = 75.7%, AE = 247.7) were constructed at an efficient donor/acceptor ratio of 100:1 (15:2 for cy5), respectively. The co-assembly with dicationic diarylethene derivative **1** made a photo-switchable light-harvesting system which was used for information encryption. The artificial light-harvesting system based on PET with NIR delayed fluorescence was used to lysosome-targeting imaging in HeLa cell.

Supporting Information

Supporting Information is available from the Wiley Online Library or from the author.

Acknowledgements

This work was financially supported by the National Natural Science Foundation of China (No. 22131008 and 21772100).

Conflict of Interest

The authors declare no conflict of interest.

Data Availability Statement

The data that support the findings of this study are available from the corresponding author upon reasonable request.

Keywords

dicationic derivatives, light-harvesting systems, phosphorescence energy transfer, supramolecular switches

Received: May 22, 2022
Revised: June 17, 2022
Published online:

[1] a) X.-K. Ma, Y. Liu, *Acc. Chem. Res.* **2021**, *54*, 3403; b) X. Ma, J. Wang, H. Tian, *Acc. Chem. Res.* **2019**, *52*, 738; c) T. Zhang, X. Ma, H. Wu, L. Zhu, Y. Zhao, H. Tian, *Angew. Chem., Int. Ed.* **2020**, *59*, 11206.
[2] a) Q. Peng, H. Ma, Z. Shuai, *Acc. Chem. Res.* **2021**, *54*, 940; b) S. Hirata, *Adv. Opt. Mater.* **2017**, *5*, 1700116.
[3] Kenry, C. Chen, B. Liu, *Nat. Commun.* **2019**, *10*, 2111.
[4] a) J. Wang, Z. Huang, X. Ma, H. Tian, *Angew. Chem., Int. Ed.* **2020**, *59*, 9928; b) L. Xu, L. Zou, H. Chen, X. Ma, *Dyes. Pigments* **2017**, *142*, 300; c) X.-K. Ma, W. Zhang, Z. Liu, H. Zhang, B. Zhang, Y. Liu, *Adv. Mater.* **2021**, *33*, 2007476; d) H.-J. Yu, Q. Zhou, X. Dai, F.-F. Shen, Y.-M. Zhang, X. Xu, Y. Liu, *J. Am. Chem. Soc.* **2021**, *143*, 13887; e) G. Qu, Y. Zhang, X. Ma, *Chin. Chem. Lett.* **2019**, *30*, 1809; f) X. Yang, D. Yan, *Chem. Sci.* **2016**, *7*, 4519; g) H. Nie, Z. Wei, X.-L. Ni, Y. Liu, *Chem. Rev.* **2022**, *122*, 9032.
[5] a) S. Wang, K. Gu, Z. Guo, C. Yan, T. Yang, Z. Chen, H. Tian, W.-H. Zhu, *Adv. Mater.* **2019**, *31*, 1805735; b) H. Chen, L. Xu, X. Ma, H. Tian, *Polym. Chem.* **2016**, *7*, 3989; c) W.-L. Zhou, Y. Chen, Q. Yu, H. Zhang, Z.-X. Liu, X.-Y. Dai, J.-J. Li, Y. Liu, *Nat. Commun.* **2020**, *11*, 4655; d) Y. Zhang, C. Zhang, Y. Chen, J. Yu, L. Chen, H. Zhang, X. Xu, Y. Liu, *Adv. Opt. Mater.* **2022**, *10*, 2102169; e) Z. Huang, Y. Hu, X. Jin, Y. Zhao, J. Su, X. Ma, *Adv. Opt. Mater.* **2021**, *9*, 2100135; f) S. Garain, S. Sarkar, B. C. Garain, S. K. Pati, S. J. George, *Angew. Chem., Int. Ed.* **2022**, *61*, e202115773; g) S. Kuila, S. Garain, S. Bandi, S. J. George, *Adv. Funct. Mater.* **2020**, *30*, 2003693.
[6] a) X.-F. Wang, W.-J. Guo, H. Xiao, Q.-Z. Yang, B. Chen, Y.-Z. Chen, C.-H. Tung, L.-Z. Wu, *Adv. Funct. Mater.* **2020**, *30*, 1907282; b) X.-F. Wang, H. Xiao, P.-Z. Chen, Q.-Z. Yang, B. Chen, C.-H. Tung, Y.-Z. Chen, L.-Z. Wu, *J. Am. Chem. Soc.* **2019**, *141*, 5045.
[7] a) X. Yu, W. Liang, Q. Huang, W. Wu, J. J. Chruma, C. Yang, *Chem. Commun.* **2019**, *55*, 3156; b) G. Farias, C. A. M. Salla, M. Aydemir, L. Sturm, P. Dechambenoit, F. Durola, B. de Souza, H. Bock, A. P. Monkman, I. H. Bechtold, *Chem. Sci.* **2021**, *12*, 15116; c) S. Garain, S. Kuila, B. C. Garain, M. Kataria, A. Borah, S. K. Pati, S. J. George, *Angew. Chem., Int. Ed.* **2021**, *60*, 12323.
[8] a) Y. Deng, P. Li, J. Li, D. Sun, H. Li, *ACS Appl. Mater. Interfaces.* **2021**, *13*, 14407; b) C. Wang, Y. Chen, Y. Xu, G. Ran, Y. He, Q. Song, *ACS Appl. Mater. Interfaces.* **2020**, *12*, 10791.
[9] H. Nie, Z. Wei, X.-L. Ni, Y. Liu, *Chem. Rev.* **2022**, *122*, 9032.
[10] a) Y. Gong, H. Chen, X. Ma, H. Tian, *ChemPhysChem* **2016**, *17*, 1934; b) T. Li, X. Ma, *Dyes. Pigments.* **2018**, *148*, 306.
[11] a) H. Gao, X. Ma, *Aggregate* **2021**, *2*, e116; b) D. A. Xu, Q. Y. Zhou, X. Dai, X. K. Ma, Y. M. Zhang, X. Xu, Y. Liu, *Chin. Chem. Lett.* **2021**, *33*, 851.
[12] a) Q. Dang, Y. Jiang, J. Wang, J. Wang, Q. Zhang, M. Zhang, S. Luo, Y. Xie, K. Pu, Q. Li, Z. Li, *Adv. Mater.* **2020**, *32*, 2006752; b) L. Zhang, R. Zhang, P. Cui, W. Cao, F. Gao, *Chem. Commun.* **2013**, *49*, 8102; c) F.-F. Shen, Y. Chen, X. Dai, H.-Y. Zhang, B. Zhang, Y. Liu, Y. Liu, *Chem. Sci.* **2021**, *12*, 1851; d) Y. Zhao, L. Ma, Z. Huang, J. Zhang, I. Willner, X. Ma, H. Tian, *Adv. Opt. Mater.* **2022**, *10*, 2102701; e) W.-L. Zhou, W. Lin, Y. Chen, X.-Y. Dai, Z. Liu, Y. Liu, *Chem. Sci.* **2022**, *13*, 573.
[13] S. Garain, B. C. Garain, M. Eswaramoorthy, S. K. Pati, S. J. George, *Angew. Chem., Int. Ed.* **2021**, *60*, 19720.
[14] M. Huo, X.-Y. Dai, Y. Liu, *Small* **2022**, *18*, 2104514.
[15] M. Huo, X.-Y. Dai, Y. Liu, *Angew. Chem. Int. Ed.* **2021**, *60*, 27171.
[16] C. Wang, X.-K. Ma, P. Guo, C. Jiang, Y.-H. Liu, G. Liu, X. Xu, Y. Liu, *Adv. Sci.* **2022**, *9*, 2103041.
[17] J. Liu, C. S. Y. Tan, O. A. Scherman, *Angew. Chem., Int. Ed.* **2018**, *57*, 8854.
[18] Y. Li, C. Qin, Q. Li, P. Wang, X. Miao, H. Jin, W. Ao, L. Cao, *Adv. Opt. Mater.* **2020**, *8*, 1902154.
[19] K.-P. Wang, Y. Chen, Y. Liu, *Chem. Commun.* **2015**, *51*, 1647.
[20] X.-M. Chen, Y. Chen, Q. Yu, B.-H. Gu, Y. Liu, *Angew. Chem., Int. Ed.* **2018**, *57*, 12519.
[21] F. Lin, H. Wang, Y. Cao, R. Yu, G. Liang, H. Huang, Y. Mu, Z. Yang, Z. Chi, *Adv. Mater.* **2022**, *34*, 2108333.
[22] G. Naren, W. Larsson, C. Benitez-Martin, S. Li, E. Pérez-Inestrosa, B. Albinsson, J. Andréasson, *Chem. Sci.* **2021**, *12*, 7073.